Heterocyclic Letters
Vol. 15| No.2|405-419|Feb-April|2025
ISSN : (print) 2231–3087 / (online) 2230-9632
CODEN: HLEEAI
http://heteroletters.org

FABRICATION OF GRAPHENE OXIDE-REINFORCED COMPOSITE POLYMERS FROM BIODEGRADABLE RESINS INCORPORATED WITH STYRENE AND METHYL METHACRYLATE MONOMERS FOR ENHANCED MECHANICAL STRENGTH

Newton Balakrishnan Mercy Eben [1], R. Nalini Suja [2], Justus Shakina[1*], P. Tharmaraj[3], Jebasingh Bhagavathsingh,[4*]

[1] Register Number: 17231242032013, Department of Chemistry, Sarah Tucker College (Affiliated to Manonmaniam Sundaranar University), Tirunelveli-627 007, Tamil Nadu, India
[2]Department of Chemistry, Panimalar Engineering College, Chennai.
[3]PG and Research Department of Chemistry, Thiagarajar College, Madurai.
[4]Department of Applied Chemistry, Karunya Institute of Technology and Sciences, Coimbatore, Tamil Nadu, India
shakina@sarahtuckercollege.edu.in, jebasinghb@karunya.edu

Abstract
Polymers are versatile materials with built-in properties. Plastics replacing metals, packaging materials and yarn materials in almost all sectors. Most of the synthetic polymers are non-biodegradable and a threat to nature. Unlike conventional polymers, polymers from plant oil are biocompatible and sustainable. Graphene Oxide (GO) reinforced polymers enhance durability and strength by adding value in flexible electronics and energy-storing devices. The properties and the structure of prepared graphene-reinforced polymer composites were investigated using Fourier transform infrared spectroscopy (FTIR), X-ray diffraction (XRD), Thermo gravimetric analysis (TGA) and Scanning electron microscopy (SEM). The FTIR spectroscopy analysis indicates the strong interfacial interaction between GO and polymer blend matrix. The XRD and SEM analysis confirm that GO was fully incorporated into individual graphene sheets and dispersed homogeneously within the polymer matrix resulting in the enhancement of the dielectric constant. These findings provide a new insight to fabricate flexible, high-k dielectric composite as a promising material for energy storage applications.
.

Keywords
Graphene Oxide, Interpenetrating Polymer Network (IPN), Young's Modulus, Tensile Strength, Biodegradable polymer, Biocompatible.

1. Introduction

Graphene oxide reinforced polymer is a composite material that combines graphene oxide (GO) with a polymer matrix. Graphene oxide is a derivative of graphene, which is a single layer of carbon atoms arranged in a two-dimensional honeycomb lattice [I]. GO is an oxidized

form of graphene, containing oxygen-containing functional groups such as epoxide, hydroxyl, and carboxyl groups on its surface [II]. The combination of graphene oxide with a polymer matrix enhances the mechanical, thermal, and electrical properties of the resulting composite material. The polymer matrix can be made from various types of polymers, such as epoxy, polyethene, polypropylene, and polystyrene, depending on the specific application and desired properties [III].

Benefits of graphene oxide reinforced polymer composites include [IV]: a) Increased mechanical strength: Graphene oxide's high surface area and exceptional mechanical properties, when dispersed within the polymer matrix, can significantly enhance the composite's tensile strength, stiffness, and impact resistance [V], b) Improved thermal conductivity: Graphene oxide has excellent thermal conductivity, and when integrated into the polymer matrix, it can enhance the composite's ability to conduct heat, making it useful in applications where thermal management is critical [VI], c) Enhanced electrical properties [VII]: Graphene oxide has semiconducting behaviour, and its incorporation into polymers can impart electrical conductivity to the composite, making it suitable for applications in electronics and sensors [VIII], d) Lightweight: Graphene oxide is incredibly lightweight, and its addition to the polymer matrix helps maintain the low weight of the composite material while adding strength and stiffness [IX], e) Barrier properties [X]: The presence of graphene oxide can improve the gas and liquid barrier properties of the polymer, making the composite material suitable for packaging and membrane applications [XI], f) Corrosion resistance: The use of graphene oxide in polymer composites can enhance the material's resistance to corrosion and chemical degradation [XII], g) Applications of graphene oxide reinforced polymer composites are diverse and include aerospace components, automotive parts, sports equipment, electronics, coatings, and biomedical devices, among others [XIII].

It is important to note that the successful incorporation of graphene oxide into a polymer matrix requires proper dispersion techniques and interfacial bonding to achieve the desired mechanical and functional properties. Researchers continue to explore various processing methods and optimization techniques to fully exploit the potential of these advanced composite materials. Herein we report the novel synthesis of graphene oxide nanosheets reinforced with the resin prepared from the vegetable oils wastes to enhance the mechanical stability of the waste materials [XIV].

2. Experimental Section GO reinforced Polymer

2.1 Synthesis of GO reinforced Polymer

The graphite natural powder (1gm) was mixed in the 40 mL of conc. H_2SO_4 (98%) under ice-cooled temperature and stirred for 30 mins. To the solution, $NaIO_4$ (12 gm) was added portion-wise for the period of 4 hrs at 0 ºC under vigorous stirring. The resulting thick, grey mass was cooled to -5 ºC and diluted with the addition of 150 mL of cooled Milli-Q water under constant stirring for 24 hrs. The colour of the solution was changed from grey to dark brown with the iodine vapours. After cooling to 0 ºC again, 5 mL of H_2O_2 (30 %) was added dropwise and stirred for 1 h, followed by the addition of Conc. HCl (5 mL). The dark brown solution was centrifuged to isolate the GO nanosheets. The resulting residue was washed thrice with ethanol (50 mL) and followed by diethyl ether (3 x 50 mL). The free-flow dark brown GO nanosheets were obtained in good yield and stored in the desiccator (Yield: 78 %).

2.1.1 Synthesis of Hydroxylated oils

Triglyceride oil (100 mL) and formic acid (100 mL) are mixed in the 1:1 *v/v* ratio under vigorous stirring at 0 °C in a beaker. To this mixture, hydrogen peroxide (30 %, 55 mL) was added slowly and continued stirring for 24 hours. The temperature of the reaction was maintained below 35 °C throughout the reaction. The resulting residue was extracted thrice

with diethyl ether (3 x 40 mL). The organic layer was separated and dried over anhydrous sodium sulphate. The solvent was filtered and evaporated using rota evaporator to isolate the hydroxylated triglyceride oil. The yellow resin was isolated with 98 % yield.

2.1.2 Synthesis of Pristine resins

Hydroxylated triglyceride oil (100 mL) was taken in an RB flask and blended with maleic anhydride (49 gm, 0.5 mol) in ambient temperature using an overhead stirrer. The mixture was heated to 70 ºC for 2 hrs and then the catalytic amount of morpholine base (3-4 drops) was added. The triglyceride oil macro monomer resin (pristine resin) was formed upon vigorous blending as a dark yellow colour highly viscous liquid.

2.2 Preparation of VPGO Polymer

Free radical catalysed addition polymerization of the pristine resins, triglyceride macro monomer resin (Cotton Seed resins) with monomers styrene (equal amount of resin 1 10mL with equal number of monomers 1 e.g., 10mL Cotton Seed resin + 10mL monomer Styrene + 0.4 g GO) was treated with the catalytic amount of benzoyl peroxide as a free radical initiator and N, N-dimethylaniline (2-3 drops) as an accelerator. After vigorous stirring for 10 min using over-head stirrer, it was poured in a glass plate mold pre-coated with silicone oil in the size of 10 x 10 cm. After 5 hours, the desired polymer sheet was peeled off from the glass plate.

2.3 Preparation of COPGO Polymer

Free radical catalysed addition polymerization of the pristine resins, triglyceride macro monomer resin (Cotton Seed resin) with monomers styrene and methyl methacrylate (Equal amount of Cotton seed resin with an equal amount of monomer 1 and monomer 2 with 0.4 g GO eg. 10mL Cotton Seed resin + 5mL monomer Styrene + 5mL monomer Methyl Methacrylate + 0.4 g GO) was treated with the catalytic amount of benzoyl peroxide as a free radical initiator and N, N-dimethylaniline (2-3 drops) as an accelerator. After vigorous stirring for 10 min using an over-head stirrer, it was poured into a glass plate mold pre-coated with silicone oil in the size of 10 x 10 cm. After 5 hours, the desired polymer sheet was peeled off from the glass plate.

2.4 Interpenetrating Polymer Network Preparation (IPNGO)

Interpenetrating Polymer Network (IPN) was obtained by blending of triglyceride macro monomer of two pristine resins, pungam resin and cotton seed resins (1:1 ratio) with the monomers of styrene and methyl methacrylate (1:1 ratio) and 0.4g of graphene oxide. The mixture of monomers and resins was vigorously blended using an overhead stirrer. A catalytic amount of benzoyl peroxide with accelerator *N, N*-dimethylaniline (2-3 drops) and 2 drops of ethylene glycol Di methacrylate as a cross-linker were added to the resulting mixture with constant stirring. The resulting mixture was stirred for 10 min and poured into a glass plate pre-coated with silicone oil. After 5 hours the polymer sheet was peeled off as a flexible IPNGO polymer sheet. (Equal amount of resin 1 and resin 2 with equal amount of monomer 1 and monomer 2 with 0.4 g GO, E.g., 10 mL Pungam resin + 10 mL Cotton Seed resin + 10 mL monomer Styrene + 10 mL monomer Methyl Methacrylate + 0.4 g GO)

2.4 Materials and Methods

The chemicals such as Conc. H_2SO_4, H_2O_2 (30 %), were purchased from Sigma-Aldrich and Conc. HCl, Diethyl ether, KCl, were purchased from Merck India and the solvents were used without further purification. Pungam Oil and Cotton Seed Oil were purchased from Merck with the purity of 97%. Formic Acid, H_2O_2 (30%), diethyl ether, anhydrous sodium sulphate, Maleic anhydride (> 99%), Morpholine (> 99.5%) and styrene (> 99%) were purchased from Sigma Aldrich. Methyl methacrylate (MMA), Benzoyl peroxide (Loba), *N, N*-dimethylaniline (Loba), and silicone oil (Loba) were used as such from the suppliers. FT-IR analysis was carried out with the spectral range of 400-4000 cm^{-1} using the IR-Prestise-21 Shimadzu instrument. The absorbance was recorded at 200-800 nm using Perkin Elmer Lambda 35 UV-

Vis spectrophotometer. The XRD patterns for polymeric materials were recorded on a Shimadzu XRD- 6000 Powder X-Ray diffractometer at 40 kV voltages and 30 mA current. All the spectra were acquired at a pressure using an ultra-high vacuum with Al Kα excitation at 250W. Scanning electron microscope (SEM) images were measured by the Hitachi S4800 field emission SEM system. TGA measurements were carried out under an N_2 atmosphere using NETZSCH STA 449 F3 Jupiter. ^{1}H and ^{13}C-NMR spectra were recorded in the deuterated solvents in Bruker NMR 300 MHz Magnet and console system. The Tensile Strength of the as-prepared copolymers were conducted in TNC universal testing computerized UTM 50 kN.

3. Result and Discussion

The GO-reinforced polymer sheets were synthesized from their respective resins, and blended with the monomers of styrene and/or MMA using benzoyl peroxide as a free radical initiator and *N*, *N*-dimethylaniline as an accelerator.

3.1 IR Spectra

The FT-IR spectra were performed to analyze the modifications in the functional groups due to the GO enforcement with the polymeric matrix. FT-IR spectra of VPGO, COPGO and IPNGO are shown in Figure 1. The broad peak appears at 3351, 3350, and 3367.8 cm^{-1} in the VPGO, COPGO and IPNGO materials [XV], respectively corresponding to the –OH $_{str}$ vibrations from the intercalated GO basal planes. The significant peaks at 1700 cm^{-1}, 1523 cm^{-1} and 1027 cm^{-1} for VPGO were responsible for the stretching vibrations from C=O $_{str}$, C=C, (-OH), and C-O-C functional groups, respectively. These results confirm the epoxy ring opening due to the nucleophilic attack of the hydroxyl group for the formation of the C-O bond. The peak at 1026 cm^{-1} was attributed to the -C-OH stretching vibration of primary alcohol. In the case of COPGO also shows intensive peaks 1698 cm^{-1}, 1509 cm^{-1} and 1081 cm^{-1}, were attributed corresponding to amide C=O, aromatic C=C bending, OH bending and C-O stretching vibrations. Meanwhile, the broad peak at 3490 cm^{-1}, corresponds to the stretching vibrations of –OH and the peak 1082 cm^{-1} is assigned to the –C-OH stretching vibration of primary alcohol [XVI].

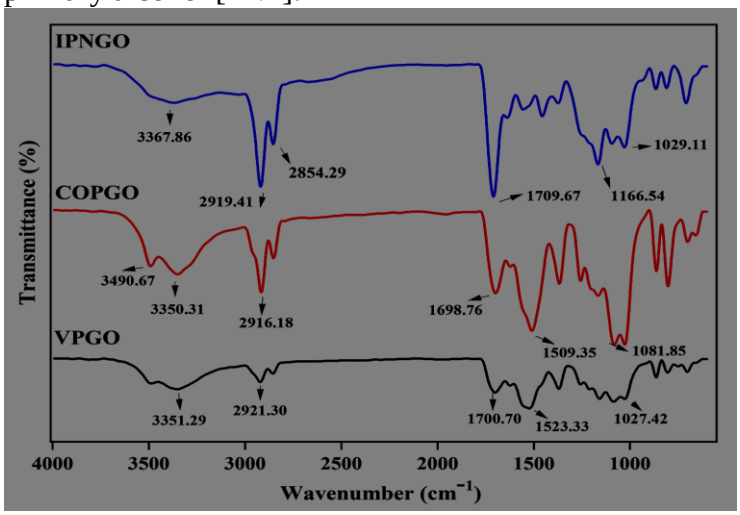

Figure 3.1: The FT-IR spectra of VPGO, COPGO and IPNGO GO-polymeric composites.

3.2 UV Spectra

The degree of polymerization in the homogeneous solution of the as-prepared resins was analyzed by the UV spectra. The UV spectra of pristine resins show strong absorption peaks around 246 nm due to the π - π^* transitions existing in the lipidic chain and the shoulder peaks around 314 nm correspond to the n-π^* transitions present in the pristine resins. Due to the

interpenetration of monomers into the resins, the solubility of GO-reinforced polymers differs from their corresponding resins in the organic solvents. It also confirms the embedding of GO in the polymer [XVII]. The UV spectra of hydroxylated oils (Fig 3.2) [XVIII].

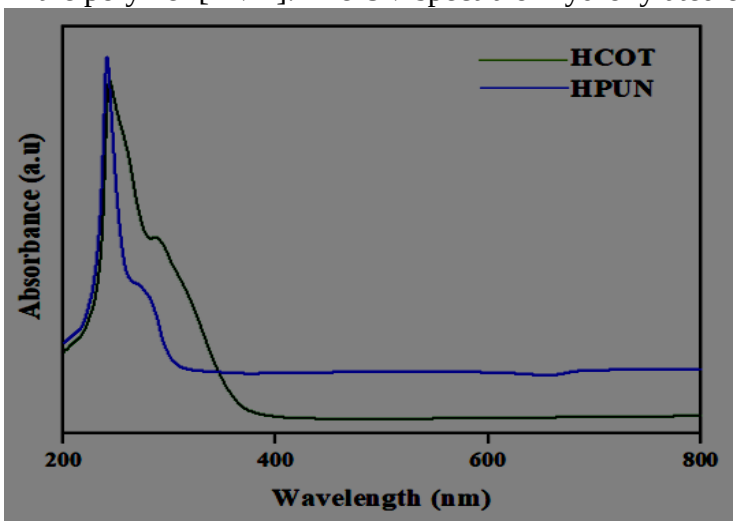

Figure 3.2: The UV-Vis spectra of hydroxylated oils of cottonseed (HCOT), and Pungam oils (HPUN).

3.3 XRD Patterns

The powder XRD analysis was performed to study the crystallinity nature of the as-prepared intercalated COPGO nanosheets and the impact of intercalation on their GO interlayer *d*-spacing. The XRD pattern of the as-prepared nanosheets and GO is shown in Figure 3. Upon intercalation, the COPGO nanosheets display the enhancement of interlayer *d*-spacing of 5.2 Å with the corresponding 2θ value of 19.69 deg. The case of highly dispersed GO nanosheets shows the interlayer spacing of 10.17 Å with the 2θ value of 8.7 deg. The decreased interlayer *d*-spacing of around 5 nm confirms the polymeric reinforcement between the basal planes of GO. It is noteworthy to report that the appearance no significant peak at 20 values of around 26 deg. for reduced GO because of polymerization [XIX].

Using Bragg's law, the interlayer *d*-spacing value of COPGO nanosheets was theoretically found to be 4.86 nm and for the GO nanosheets the value of 0.93 nm with the increase of around 1.3 nm compared with the pristine graphene oxide. The full-width half maximum (FWHM) value of the diffraction peak in the XRD pattern of the COPGO nanosheets was found to be much higher than the corresponding value of the precursor. The mean crystallite thickness of as-prepared GO nanosheets was calculated using the Debye-Scherrer equation (Equation 01).

$$t = K\lambda/FWHM \cos\theta \quad \text{…….....} \quad \text{(Eqn. 1)}$$

where t is the mean crystallite thickness K is a dimensionless shape factor with a value of about 0.9 λ is the wavelength of the X-ray used (λ-1.5418) θ is the angular position of the peak and FWHM is the full width at half maximum obtained from the graph (expressed in radians). The value of the average crystallite thickness for graphene oxide is ~7 Å and for COPGO nanosheets was around 4-5 Å. The number of functionalized GO layers containing heteroatoms N-considering the using the equation 2.

$$N = t/d \quad \text{.....……} \quad \text{(eqn. 2)}$$

Where t is the crystallite thickness, d is the lattice spacing and the number of layers for **COPGO** tOH is ~ 4 layers.[22,23]

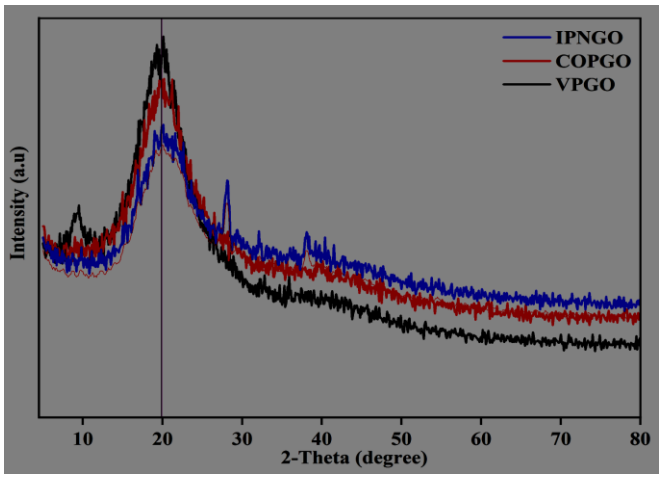

Figure 3.3: The Powder XRD patterns of VPGO, COPGO and IPNGO GO-polymeric composites

3.4 SEM Images

The surface morphology and the microstructure of the GO-polymeric composites were investigated by the SEM analysis [XX]. The SEM images of VPGO, COPGO and IPNGO are given in figure 3.4. The functionalized GO shows a wrinkled surface with a sheet-like structure due to the intercalation on the GO basal planes. The as-prepared sheets were flatly deposited and occasionally folded without neither coagulation nor aggregation [XXI] [XXII].

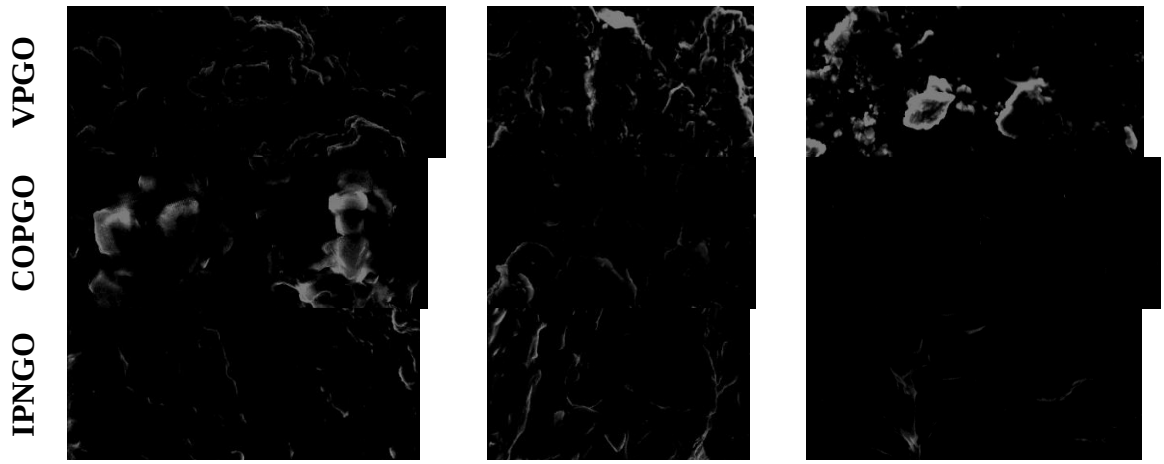

Figure 3.4: The SEM Images of VPGO, COPGO and IPNGO GO-polymeric composites

3.5 Thermal Properties

The thermal stability of the as-prepared GO-polymeric composites was analyzed by thermogravimetric and thermo analytical techniques with the increase of linear temperature [XXIII]. The thermogravimetric curves of as-prepared copolymers show enhanced thermal stability due to the formation of block copolymers from their corresponding two monomers (Fig. 3.5) [XXIV], whereas the biodegradable triglyceride hydroxylated oils and its pristine resin were decomposed at around 280 °C. The weight loss of the pungam oil copolymer displays around 20 % weight loss at 110 ºC compared to the other two copolymers due to the release of hydrated molecules [XXV]. Typically, the hydrated molecules were found to be very low in the case of sunflower and cottonseed oil. The as-prepared copolymers show the thermal decomposition curves at 340-410 °C with around 69 % weight loss, which was mainly due to the decomposition of hydrocarbons and carboxylic acid moieties [XXVI].

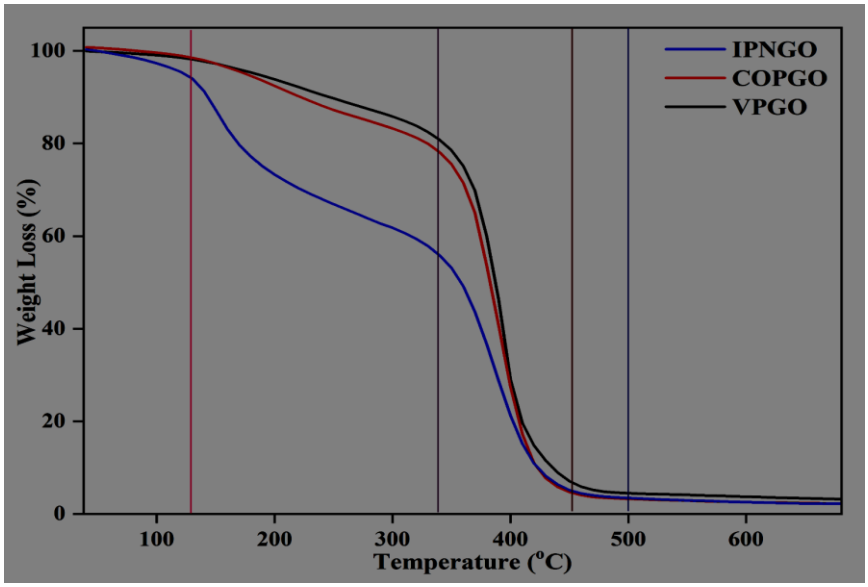

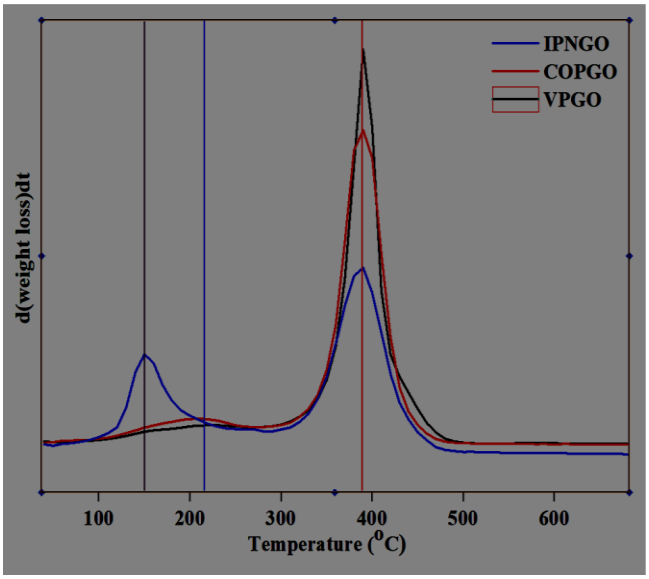

Figure 3.5. (a) Thermogravimetric analysis of VPGO, COPGO and IPNGO composites, (b) DSC graphs, (c) DTA and (d) Stress-Strain graph of VPGO, COPGO and IPNGO di-block copolymers, respectively.

The DSC analysis was executed to analyze the variation of heat flow of prepared GO-polymeric composites with variation of temperature up to 700 ºC. Their corresponding DSC graphs were shown in Fig. 3.5. From the DSC curves, the glass transition temperature (T_g) of copolymers exhibits in the range of 133-175 °C which corresponding to the reversible transition to viscous state. In the case of pungam based copolymer shows the significant glass transition temperature of 133 ºC attributed to the enhanced viscous state [XXVII]. The as-prepared copolymers show

thermal endotherm at 365-395 ºC corresponding to the formation of the polymeric matrix. It confirms the blending of two monomers with the corresponding resins yields concordant thermal transitions at high heat flow differences with the formation of an enhanced degree of crystallinity and thermal stability of biodegradable polymers. It is noteworthy to report that the existence of one T_g of copolymers is due to the homo-phasic nature of chemically identical resins with differing molecular masses [XXVIII].

To study the degradation patterns of the as-prepared polymeric GO composites, differential thermal analysis (DTA) was performed with various temperatures with respect to their rate of change of mass. Their corresponding DTA curves were shown in the Figure 3.5. The DTA curves revealed that the prepared GO reinforced copolymers underwent the uniform degradation in terms of weight loss with the increase of temperature. At low temperatures, the copolymers undergo the removal of volatile substances and the degradation of inter-crossed thermostable structures was observed at the temperature 370-390 ºC. Above 500 ºC temperature, the maximum rate of degradation was obtained due to the blending of two monomers into the pristine resins from the vegetable oils [XXIX].

3.6 Mechanical Properties

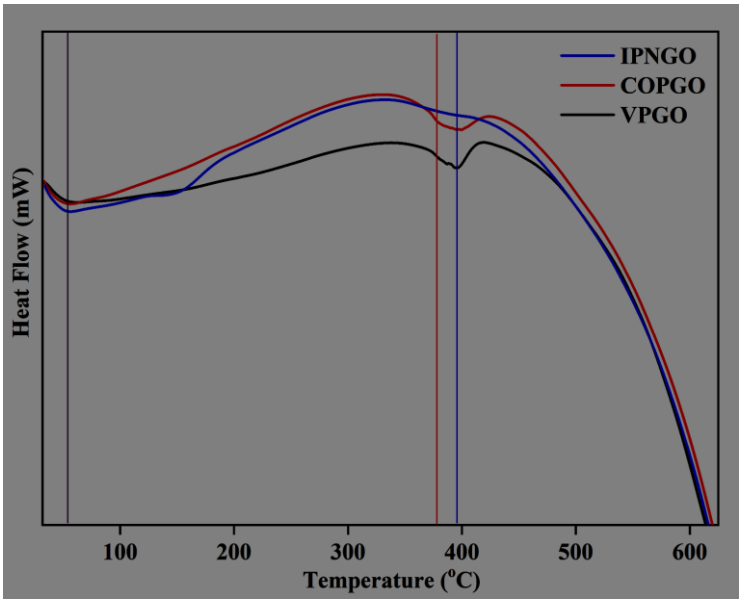

The respective stress and strain were determined for the GO-reinforced polymers VPGO, COPGO and IPNGO to calculate the young's moduli, by applying stress along the longitudinal axis and the observed deformations were measured along the same axis. The stress-strain graph that compares the mechanical properties of the GO-reinforced polymers is demonstrated in Figure 3.6 [XXX]. below. It is observed that enhanced Young's modulus is obtained for VPGO polymer. Compared to COPGO and IPNGO, VPGO showed better stability [XXXI]. Young's Modulus was calculated and is given below in Table 1. VPGO exhibited a high tensile strength of 104.69 kg/cm^2 while IPNGO showed the least of 4.35 kg/cm^2. The high tensile strength of COPGO allowed it to have a high elongation percentage at a break of 39.2% thus making it more desirable and loftier, comparatively [XXXII]. Also, it is observed from the graph that after reaching a certain point the value of stress dropped drastically in the case of IPNGO and COPGO. IPNGO has higher yield strength exhibiting brittle properties while COPGO and IPNGO, are ductile with lesser yield strength. Lease fracture strength is shown by IPNGO having an elongation break of 4.743% [XXXIII]

GO reinforced polymer	Tensile Strength (kg/cm^2)	Elongation at break %	Young's Modulus (MPa)
VPGO	104.69	39.2	107.2
COPGO	54.88	35.97	149.6
IPNGO	4.35	4.74	89.9

Table 3.6: The mechanical strength of VPGO, COPGO and IPNGO polymers, respectively.

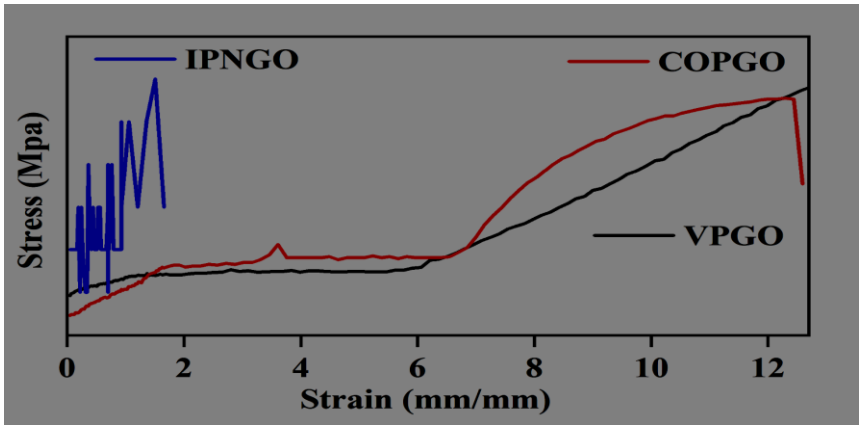

Figure 3.6: The Stress-Strain graph of VPGO, COPGO and IPNGO polymers, respectively.

3.7 Biodegradation of GO reinforced Polymer

Biodegradation of thermosetting GO-reinforced polymer is evaluated by soil burial tests. The specimens VPGO, COPGO and IPNGO are buried in fertile soil, the distance from the samples to the soil surface is around 10 cm for one month. The Optical Images and the weight loss are measured and compared for individual samples before and after burial. The degradation rate of GO-reinforced polymer is superior to biodegradation than its corresponding Petro-based polymer [XXXIV].

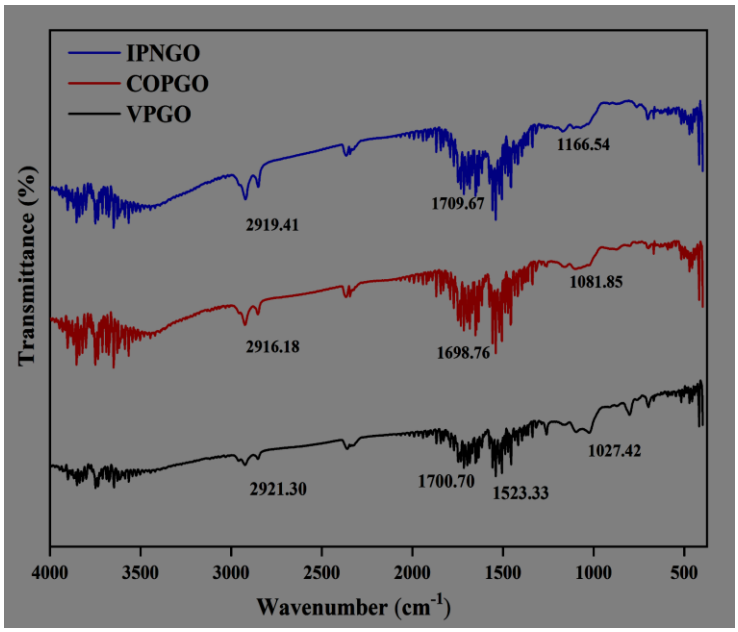

Figure 3.7: The FT-IR spectra of the samples VPGO, COPGO and IPNGO GO-polymeric composite after the burial test and weight of the respective composites.

Table 3.7

Sample Name	VPGO	COPGO	IPNGO
Before Soil Burial	0.781g	0.584g	0.275g
After Soil Burial	0.630g	0.434g	0.154g
Weight Reduced	0.151g	0.150g	0.121g

Table 3.7: The weight of VPGO, COPGO and IPNGO polymers before and after burial test respectively.

In soil burial degradation, the entire morphology of the polymer film changes upon degradation for all polyesters [XXXV]. Stains were also observed which are suspected evidence that polymer samples are degraded by the attack of microorganisms in the soil. Microorganisms such as bacteria, fungi and actinomycetes are involved in the degradation of both natural and synthetic plastics [XXXVI]

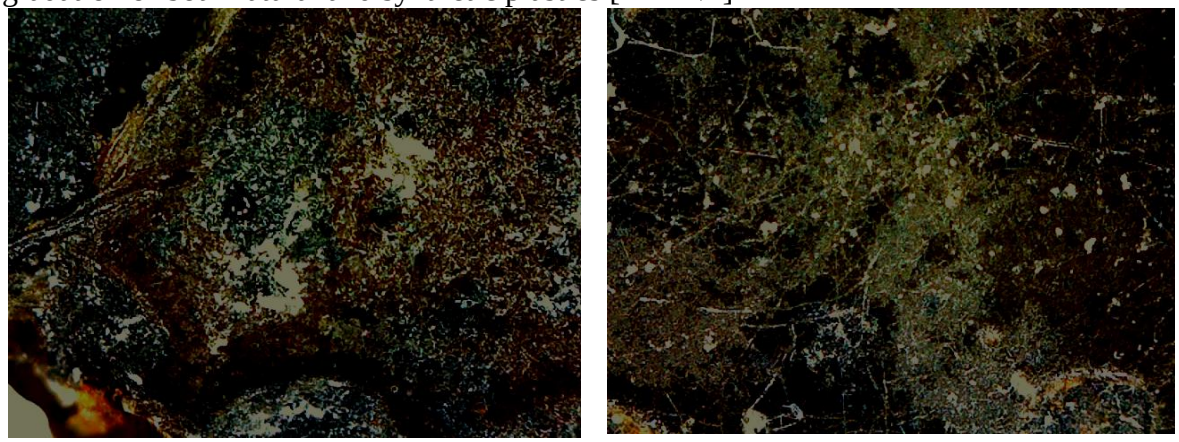

Fig.3.7.1. The Optical Images of VPGO polymeric composite before and after burial test

.

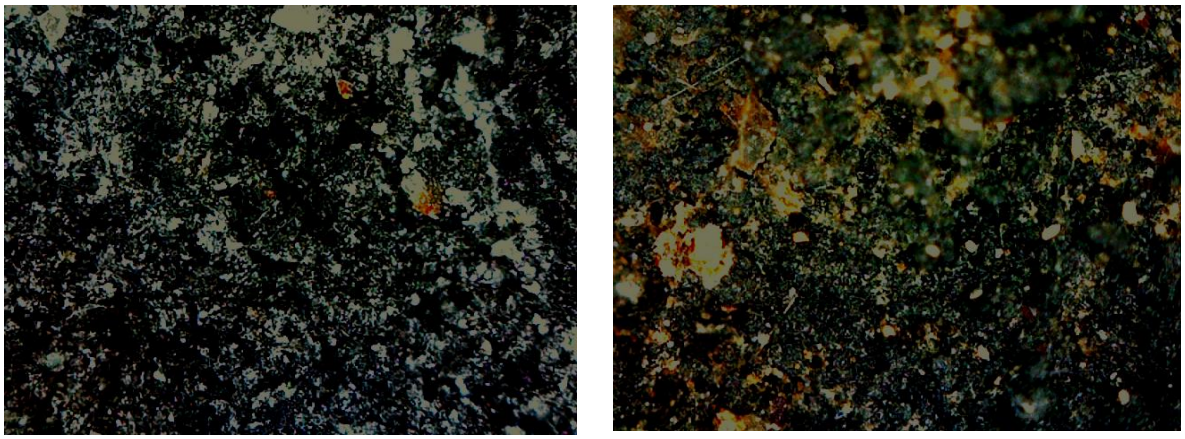

Fig.3.7.2. The Optical Images of COPGO polymeric composite before and after burial test.

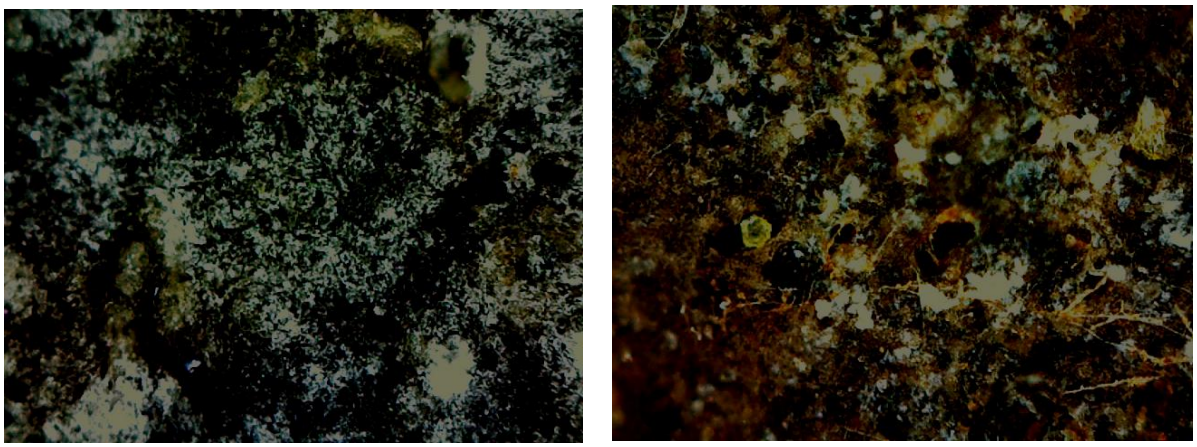

Fig.3.7.3. The Optical Images of IPNGO polymeric composite before and after burial test

3.8 Comparative Study Of VPGO, COPGO And IPNGO Composites

The comparative analysis of VPGO, COPGO, and IPNGO composites highlights the exceptional properties of VPGO, positioning it as a highly desirable material for electrode applications stands out due to its high dielectric constant, showcasing excellent electrical properties crucial for electrode materials. Moreover, its impressive mechanical and thermal characteristics further contribute to its suitability for such applications. The significant tensile strength of VPGO at 104.69 kg/cm^2 is a key factor that sets it apart. This high tensile strength allows VPGO to exhibit a remarkable elongation percentage at break (39.2%), making it more flexible and resilient compared to IPNGO and COPGO. Flexibility is a crucial aspect for electrode materials, as they may undergo mechanical stresses during usage, and VPGO's ability to withstand such stresses is a considerable advantage. The observed stress-strain graph patterns reveal that VPGO maintains a stable stress level without the drastic drop seen in IPNGO and COPGO. This behaviour suggests that VPGO possesses better durability and reliability under varying stress conditions, a crucial aspect for sustained performance as an electrode material. Furthermore, the glass transition temperature of 133 ºC in the VPGO-based polymer indicates enhanced thermal stability, an essential feature for materials used in electrodes, especially when subjected to temperature variations during operation. In contrast, IPNGO, despite having higher yield strength, exhibits brittle properties, which may limit its applicability as an electrode material. The lower fracture strength and elongation at break of IPNGO (4.743%) further emphasize its inferior flexibility compared to VPGO. In conclusion, the comprehensive analysis suggests that VPGO, with its combination of high dielectric constant, impressive mechanical properties, and significant glass transition temperature, is a standout candidate for electrode materials. Its flexibility, durability, and thermal stability make it a superior choice, providing a strong foundation for the selection of VPGO as a promising material for electrode applications.

Conclusions

The GO-reinforced polymeric composites were prepared and characterised by both spectroscopic and microscopic techniques to explore the structural modification on the basal planes due to the enforcement of the polymeric matrix. The hydrophilicity of the intercalated GO nanosheets was enhanced due to the OH groups present in the polymeric structure. IR, PXRD, and UV confirm the polymeric interaction with the hydrophilic interaction of the surface of GO basal planes. After the functionalized GO nanosheets with polymeric monomers show a high dispersion in the solvent. The interlayer *d*-spacing was decreased due to the insertion of the polymeric composites on the GO surface through the ring opening of epoxy

groups in the GO sheets. Furthermore, imino alcohol functionalized GO may considerably enhance the wettability of the material interaction due to the heteroatom (-OH) decoration. The design and development of intercalated nanosheets are certainly proven for the enhancement of GO layers and could be used as an electrode material for biological fluid-based sensor applications.

Acknowledgement
The authors thank the HPLC MASS Facility and NMR Facility at the Department of Applied Chemistry, Karunya Institute of Technology and Sciences, Coimbatore for the characterization of the polymer samples. The authors thank the Department of Chemistry, Sarah Tucker College for instrumentation facilities for polymer synthesis. The author's sincere thanks to DST-CURIE (DST/CURIE-PG/2022/91 (G)) and DST-FIST for providing software, analytical and infrastructure facilities at the Department of Chemistry and Research Centre, Sarah Tucker College (Autonomous), Tirunelveli-627 007.

Ethical Approval: Not Applicable
Competing Interests: Not Applicable
Authors Contributions:
Newton Balakrishnan Mercy Eben: Experiments, Data Collections, First Draft
Justus Shakina: Conceptualization, Experiment design, Drafting and Reviewing
Jebasingh Bhagavathsingh: Conceptualization, Supervision, Drafting, Reviewing
Funding: This study did not receive any funding in any form.
Data Availability Statement: The data used to support the findings of this study are included within the supplementary information file.
Conflict of interest: The authors declare no conflicts of interest.
Supplementary Materials: The figures of UV, FT-IR and ^{1}H-NMR spectra of Hydroxylated plant oils were given as supplementary materials.

References

I. Abdullah, S. I., & Ansari, M. N. M. (2020). Preparation and characterization of electrical properties of graphene oxide (GO)/epoxy composites. *Materials Today: Proceedings*, *20*(xxxx), 474–477. https://doi.org/10.1016/j.matpr.2019.09.169

II. Arumugam, H., Krishnasamy, B., Perumal, G., A, A. D., Abdul Aleem, M. I., & Muthukaruppan, A. (2021). Bio-composites of rice husk and saw dust reinforced bio-benzoxazine/epoxy hybridized matrices: Thermal, mechanical, electrical resistance and acoustic absorption properties. *Construction and Building Materials*. https://doi.org/10.1016/j.conbuildmat.2021.125381

III. Belaid, H., Nagarajan, S., Teyssier, C., Barou, C., Barés, J., Balme, S., Garay, H., Huon, V., Cornu, D., Cavaillès, V., & Bechelany, M. (2020). Development of new biocompatible 3D printed graphene oxide-based scaffolds. *Materials Science and Engineering C*, *110*. https://doi.org/10.1016/j.msec.2019.110595

IV. Costa, U. O., Nascimento, L. F. C., Garcia, J. M., Bezerra, W. B. A., Fabio da Costa, G. F., Luz, F. S. da, Pinheiro, W. A., & Monteiro, S. N. (2020). Mechanical properties of composites with graphene oxide functionalization of either epoxy matrix or curaua fiber reinforcement. *Journal of Materials Research and Technology*, *9*(6). https://doi.org/10.1016/j.jmrt.2020.09.035

V. Fan, W., & Zheng, S. (2008). Reaction-induced microphase separation in thermosetting blends of epoxy resin with poly(methyl methacrylate)-block-polystyrene block copolymers: Effect of topologies of block copolymers on morphological structures. *Polymer*, *49*(13–14), 3157–3167. https://doi.org/10.1016/j.polymer.2008.05.010

VI. Farooq, U., Teuwen, J., & Dransfeld, C. (2020). Toughening of epoxy systems with interpenetrating polymer network (IPN): A review. In *Polymers* (Vol. 12, Issue 9). https://doi.org/10.3390/POLYM12091908

VII. Gong, L., Zhang, F., Peng, X., Scarpa, F., Huang, Z., Tao, G., Liu, H. Y., Zhou, H., & Zhou, H. (2022). Improving the damping properties of carbon fiber reinforced polymer composites by interfacial sliding of oriented multilayer graphene oxide. *Composites Science and Technology*, *224*. https://doi.org/10.1016/j.compscitech.2022.109309

VIII. Hatta, M., Shinya, A., Gomi, H., Vallittu, P. K., Säilynoja, E., & Lassila, L. V. J. (2021). Effect of interpenetrating polymer network (Ipn) thermoplastic resin on flexural strength of fibre-reinforced composite and the penetration of bonding resin into semi-ipn frc post. *Polymers*, *13*(18). https://doi.org/10.3390/polym13183200

IX. Herrera-Sandoval, G. M., Baez-Angarita, D. B., Correa-Torres, S. N., Primera-Pedrozo, O. M., & Hernández-Rivera, S. P. (2013). Novel EPS/TiO2 Nanocomposite Prepared from Recycled Polystyrene. *Materials Sciences and Applications*, *04*(03). https://doi.org/10.4236/msa.2013.43021

X. Jagadeesh, P., Puttegowda, M., Thyavihalli Girijappa, Y. G., Rangappa, S. M., & Siengchin, S. (2022). Effect of natural filler materials on fiber reinforced hybrid polymer composites: An Overview. *Journal of Natural Fibers*, *19*(11), 4132–4147. https://doi.org/10.1080/15440478.2020.1854145

XI. Joshi, G. M., & Deshmukh, K. (2014). Optimized quality factor of graphene oxide-reinforced PVC nanocomposite. *Journal of Electronic Materials*, *43*(4). https://doi.org/10.1007/s11664-014-3010-z

XII. Karimi, B., & Ramezanzadeh, B. (2017). A comparative study on the effects of ultrathin luminescent graphene oxide quantum dot (GOQD) and graphene oxide (GO) nanosheets on the interfacial interactions and mechanical properties of an epoxy

composite. *Journal of Colloid and Interface Science*, *493*. https://doi.org/10.1016/j.jcis.2017.01.013

XIII. Kavimani, V., Soorya Prakash, K., Thankachan, T., & Udayakumar, R. (2020). Synergistic improvement of epoxy derived polymer composites reinforced with Graphene Oxide (GO) plus Titanium di oxide(TiO2). *Composites Part B: Engineering*, *191*. https://doi.org/10.1016/j.compositesb.2020.107911

XIV. Kim, H., Lee, J., Shim, S. Bin, Kim, M. S., Shrimant, B., Lee, J. H., Nam, S. Y., Kwon, D. J., & Park, J. H. (2023). Influence of milled and acid-treated graphene oxide on the self-healing properties of graphene oxide reinforced polyurethane. *Composites Part B: Engineering*, *259*. https://doi.org/10.1016/j.compositesb.2023.110702

XV. Kim, S. D., Zhang, W. L., & Choi, J. (2014). *Electronic supplementary information Pickering emulsion-fabricated smart microspheres of polystyrene/graphene oxide and their electrorheology*.

XVI. Mahendran, R., Sridharan, D., Santhakumar, K., & Gnanasekaran, G. (2016). Green Route Fabrication of Graphene Oxide Reinforced Polymer Composites with Enhanced Mechanical Properties. *Journal of Nanoscience*, *2016*. https://doi.org/10.1155/2016/6410295

XVII. Mosaliganti, S., Rama Kirshna, Y., Venkatesh, M., Prasad, V. V. S., & Swetha, B. (2023). Fabrication and characterization of nano Al2O3 fiber-reinforced polymer composites. *Materials Today: Proceedings*. https://doi.org/10.1016/j.matpr.2023.03.340

XVIII. Newton Balakrishnan, M. E., Muralkar, P., Ranjana Ponraj, M., Nadiger, S., Dhandayutham, S., Justus, S., & Bhagavathsingh, J. (2022). Recycling of saw dust as a filler reinforced cotton seed oil resin amalgamated polystyrene composite material for sustainable waste management applications. *Materials Today: Proceedings*, *58*(xxxx), 783–788. https://doi.org/10.1016/j.matpr.2022.03.331

XIX. Ningaraju, S., Jagadish, K., Srikantaswamy, S., Gnana Prakash, A. P., & Ravikumar, H. B. (2019). Synthesis of graphite oxide nanoparticles and conductivity studies of PSF/GO and PSAN/GO polymer nanocomposites. *Materials Science and Engineering B: Solid-State Materials for Advanced Technology*, *246*. https://doi.org/10.1016/j.mseb.2019.06.002

XX. Pal, A. (2023). Challenges and Future Prospects. In *Polymer-Carbonaceous Filler Based Composites for Wastewater Treatment*. https://doi.org/10.1201/9781003328094-16

XXI. Pereira, A. C., Lima, A. M., Demosthenes, L. C. da C., Oliveira, M. S., Costa, U. O., Bezerra, W. B. A., Monteiro, S. N., Rodriguez, R. J. S., de Deus, J. F., & Pinheiro, W. A. (2020). Ballistic performance of ramie fabric reinforcing graphene oxide-incorporated epoxy matrix composite. *Polymers*, *12*(11). https://doi.org/10.3390/polym12112711

XXII. Rajan, S., Marimuthu, K., Balaji Ayyanar, C., Khan, A., Siengchin, S., & Mavinkere Rangappa, S. (2022). In-vitro cytotoxicity of zinc oxide, graphene oxide, and calcium carbonate nano particulates reinforced high-density polyethylene composite. *Journal of Materials Research and Technology*, *18*. https://doi.org/10.1016/j.jmrt.2022.03.012

XXIII. Rosi, F., Miliani, C., Gardner, P., Chieli, A., Romani, A., Ciabatta, M., Trevisan, R., Ferriani, B., Richardson, E., & Cartechini, L. (2021). Unveiling the composition of historical plastics through non-invasive reflection FT-IR spectroscopy in the extended near- and mid-Infrared spectral range. *Analytica Chimica Acta*, *1169*. https://doi.org/10.1016/j.aca.2021.338602

XXIV. Senis, E. C., Golosnoy, I. O., Dulieu-Barton, J. M., & Thomsen, O. T. (2019). Enhancement of the electrical and thermal properties of unidirectional carbon fibre/epoxy laminates through the addition of graphene oxide. *Journal of Materials Science*, *54*(12). https://doi.org/10.1007/s10853-019-03522-8

XXV. Shami, R., Sabir, A., Iqbal, S. S., Gull, N., Zohra, R., & Khan, S. M. (2023). Synergistic effect of GO/ZnO loading on the performance of cellulose acetate/chitosan blended reverse osmosis membranes for NOM rejection. *Heliyon*, *9*(3). https://doi.org/10.1016/j.heliyon.2023.e13736

XXVI. Sharma, B. (2020). Viscoelastic investigation of graphene oxide grafted PVA biohybrid using ostwald modeling for packaging applications. *Polymer Testing*, *91*. https://doi.org/10.1016/j.polymertesting.2020.106791

XXVII. Shuai, C., Guo, W., Wu, P., Yang, W., Hu, S., Xia, Y., & Feng, P. (2018). A graphene oxide-Ag co-dispersing nanosystem: Dual synergistic effects on antibacterial activities and mechanical properties of polymer scaffolds. *Chemical Engineering Journal*, *347*. https://doi.org/10.1016/j.cej.2018.04.092

XXVIII. Silverstein, M. S. (2020). Interpenetrating polymer networks: So happy together? *Polymer*, *207*. https://doi.org/10.1016/j.polymer.2020.122929

XXIX. Sujan, M. I., Sarkar, S. D., Roy, C. K., Ferdous, M., Goswami, A., Gafur, M. A., & Azam, M. S. (2021). Graphene oxide crosslinker for the enhancement of mechanical properties of polylactic acid. *Journal of Polymer Science*, *59*(11). https://doi.org/10.1002/pol.20210029

XXX. Tsagkalias, I. S., Vlachou, A., Verros, G. D., & Achilias, D. S. (2019). Effect of graphene oxide or functionalized graphene oxide on the copolymerization kinetics of Styrene/n-butyl methacrylate. *Polymers*, *11*(6). https://doi.org/10.3390/polym11060999

XXXI. Uppin, V. S., Gouda, P. S. S., Kittur, M. I., Andriyana, A., Ang, B. C., Parveez, B., Badruddin, I. A., Javed, S., & Kamangar, S. (2022). Mechanical Response of Glass–Epoxy Composites with Graphene Oxide Nanoparticles. *Materials*, *15*(23). https://doi.org/10.3390/ma15238545

XXXII. Vlasceanu, G. M., Crica, L. E., Pandele, A. M., & Ionita, M. (2020). Graphene oxide reinforcing genipin crosslinked chitosan-gelatin blend films. *Coatings*, *10*(2). https://doi.org/10.3390/coatings10020189

XXXIII. Wang, G., He, C., Yang, W., Qi, F., Qian, G., Peng, S., & Shuai, C. (2020). Surface-Modified Graphene Oxide with Compatible Interface Enhances Poly-L-Lactic Acid Bone Scaffold. *Journal of Nanomaterials*, *2020*. https://doi.org/10.1155/2020/5634096

XXXIV. Xiao, R., Ding, M., Wang, Y., Gao, L., Fan, R., & Lu, Y. (2021). Stereolithography (SLA) 3D printing of carbon fiber-graphene oxide (CF-GO) reinforced polymer lattices. *Nanotechnology*, *32*(23). https://doi.org/10.1088/1361-6528/abe825

XXXV. Xu, L., Zhao, J., Shi, M., Liu, J., & Wang, Z. (2022). Thermodynamic properties of TPI shape memory polymer composites reinforced by GO/SiO2 modified carbon fiber. *Composites Science and Technology*, *226*. https://doi.org/10.1016/j.compscitech.2022.109551

XXXVI. Zapata-González, I., Hutchinson, R. A., Matyjaszewski, K., Saldívar-Guerra, E., & Ortiz-Cisneros, J. (2014). Copolymer composition deviations from mayo-lewis conventional free radical behavior in nitroxide mediated copolymerization. *Macromolecular Theory and Simulations*, *23*(4), 245–265. https://doi.org/10.1002/mats.201300137

Received on April 11,2024.